

The extended halo of NGC 2682 (M 67) from Gaia DR2

R. Carrera¹, M. Pasquato¹, A. Vallenari¹, L. Balaguer-Núñez², T. Cantat-Gaudin², M. Mapelli^{1,3,4,5}, A. Bragaglia⁶, D. Bossini^{1,7}, C. Jordi², D. Galadí-Enríquez⁸, and E. Solano⁹

¹ INAF-Osservatorio Astronomico di Padova, vicolo dell'Osservatorio 5, 35122 Padova (Italy)
e-mail: jimenez.carrera@inaf.it

² Institut de Ciències del Cosmos, Universitat de Barcelona (IEEC-UB), Martí i Franquès 1, E-08028 Barcelona, Spain

³ Physics and Astronomy Department Galileo Galilei, University of Padova, Vicolo dell'Osservatorio 3, I-35122, Padova, Italy

⁴ INFN-Padova, Via Marzolo 8, I-35131 Padova, Italy

⁵ Institut für Astro- und Teilchenphysik, Universität Innsbruck, Technikerstrasse 25/8, A-6020, Innsbruck, Austria

⁶ INAF-Osservatorio di Astrofisica e Scienza dello Spazio, via P. Gobetti 93/3, 40129 Bologna, Italy

⁷ Instituto de Astrofísica e Ciências do Espaço, Universidade do Porto, CAUP, Rua das Estrelas, 4150-762 Porto, Portugal

⁸ Observatorio de Calar Alto, Sierra de los Filabres, E-04550-Gérgal (Almería), Spain

⁹ Centro de Astrobiología (INTA-CSIC), Departamento de Astrofísica. P.O. Box 78, E-28691, Villanueva de la Cañada, Madrid, Spain; Spanish Virtual Observatory

Received; accepted

ABSTRACT

Context. NGC 2682 is a nearby open cluster, approximately 3.5 Gyr old. Dynamically, most open clusters should dissolve on shorter timescales, of ≈ 1 Gyr. Having survived until now, NGC 2682 was likely much more massive in the past, and is bound to have an interesting dynamical history.

Aims. We investigate the spatial distribution of NGC 2682 stars to constrain its dynamical evolution, especially focusing on the marginally bound stars in the cluster outskirts.

Methods. We use *Gaia* DR2 data to identify NGC 2682 members up to a distance of ~ 150 pc (10 degrees). Two methods (*Clusterix* and *UPMASK*) are applied to this end. We estimate distances to obtain three-dimensional stellar positions using a Bayesian approach to parallax inversion, with an appropriate prior for star clusters. We calculate the orbit of NGC 2682 using the *GRAVPO16* software.

Results. The cluster extends up to $200'$ (50 pc) which implies that its size is at least twice as previously believed. This exceeds the cluster Hill sphere based on the Galactic potential at the distance of NGC 2682.

Conclusions. The extra-tidal stars in NGC 2682 may originate from external perturbations such as disk shocking or dynamical evaporation from two-body relaxation. The former origin is plausible given the orbit of NGC 2682, which crossed the Galactic disk ≈ 40 Myr ago.

Key words. Astrometry – Galaxy: disk – open clusters and associations: individual: NGC 2682

1. Introduction

The dynamical evolution of a stellar cluster is strongly affected by internal collisional dynamics, i.e. two-body gravitational encounters between stars (see Spitzer 1987, for an in-depth discussion in the case of globular star clusters), stellar-wind mass loss, and external interactions such as encounters with molecular clouds (Spitzer 1958; Gieles et al. 2009) or Galactic disk and spiral arms (Binney & Tremaine 1987). These phenomena modify the cluster structure and internal distribution of the stars along with its lifetime and eventually bring the cluster to dissolution. In fact, they are so effective that dynamical models predict that a cluster with the typical mass of a bound open cluster (OC), $\lesssim 10^4 M_\odot$, would be dissolved in a timescale of $\lesssim 1$ Gyr (see e.g. Baumgardt & Makino 2003; Lamers et al. 2005; Bastian & Gieles 2008).

However, about 20% of the known OCs have ages older than 1 Gyr (Dias et al. 2002; Kharchenko et al. 2013). Although they are a minority, they are key to investigate the dynamical evolution of clusters, and the balance among self gravity, internal

dynamics, and external tidal forces. These old OCs have several features that differentiate them from the bulk of the OCs population. They are systematically more massive than the younger bound clusters. In particular, although these clusters are unambiguously related to the Galactic disk because of their age and chemical composition, they are also often found at high altitude above the Galactic plane, away from the disk's disruptive influence. Even though, strictly speaking, it would be hard to exclude that some cluster have been accreted from external galaxies in merging processes.

NGC 2682 (M 67) is one of the nearest old OCs (3.6 Gyr, Bossini et al. 2019) located at about 860 pc from the Sun (Cantat-Gaudin et al. 2018a) to which it is quite similar in terms of age and initial chemical composition (e.g. Liu et al. 2016), to the point that it has long been debated whether the Sun might actually have originated from NGC 2682 (see Pichardo et al. 2012, and references therein). Evidence of substantial dynamical evolution in this cluster has been reported by several authors, such as the existence of mass segregation (e.g. Fan et al. 1996; Balaguer-Núñez et al. 2007; Bonatto & Bica

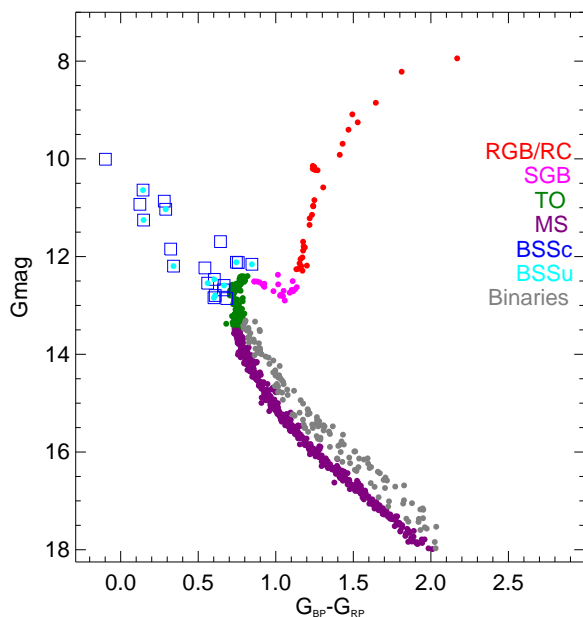


Fig. 1. *Gaia* DR2 colour-magnitude diagram of the stars labeled as members by both *UPMASK* and *Clusterix*. The different populations have been plotted in different colours: RGB/RC (red), SGB (magenta), TO (green), MS (purple), BSSc from *Clusterix* (BSSc, blue squares) and *UPMASK* (BSSu, cyan), and binaries (grey).

2003; Davenport & Sandquist 2010; Geller et al. 2015; Gao 2018) or an elongated halo roughly aligned with the cluster proper motion (Davenport & Sandquist 2010). In fact dynamical simulations of this cluster suggest that it initially was 10 times more massive (Hurley et al. 2005).

The astrometric information provided by the second data release of the *Gaia* mission, *Gaia* DR2 (Gaia Collaboration et al. 2016, 2018b) has proven a valuable tool to investigate the extra-tidal regions of several OCs in the solar neighborhood. Tidal tails have been revealed in the Hyades (Melotte 25 Meingast & Alves 2019; Röser et al. 2019), Coma Berenices (Melotte 111 Fürnkranz et al. 2019), and Praesepe (NGC 2632 Röser & Schilbach 2019) open clusters. All of them with ages younger than 1 Gyr (e.g. Bossini et al. 2019). However, hints of the existence of cluster member beyond the tidal radius have also been reported around the cluster Ruprecht 147 (Yeh et al. 2019) with an age older than 1 Gyr (e.g. Kharchenko et al. 2013).

In this paper we studied the current dynamical status of NGC 2682 using *Gaia* DR2. The observational material utilized in this paper is presented in Sect. 2. The obtained density profile is discussed in Sect. 3. The 3D spatial distribution is derived in Sect. 4 using a Bayesian approach to parallax inversion. Finally, in Sect. 5 we draw conclusions, showing that NGC 2682 is more extended than expected and that its outer envelope of extra-tidal stars may be the result of disk shocking.

2. The data

Gaia DR2 provides 5-parameter astrometric solution, i.e. positions (α and δ), proper motions (μ_{α^*} , μ_{δ}), and parallaxes (ϖ) plus magnitudes in three photometric bands (G , G_{BP} and G_{RP}) for more than 1.3 billion sources, and radial velocities (RV) for more than 7 million stars (Gaia Collaboration et al. 2018b; Katz et al. 2019; Lindegren et al. 2018). We study the data from *Gaia* DR2 in a radius of 10 deg (~ 150 pc) from the centre of NGC 2698 as determined by Cantat-Gaudin et al. (2018a): $\alpha_c=132^{\circ}846$ and

$\delta_c=11^{\circ}814$. We follow the recommendations by Arenou et al. (2018), Lindegren et al. (2018, eqs. C.1 and C.2) and *Gaia* DR2 known-issues cosmos webpage¹ for an astrometrically clean subset. We also limit our analysis to those objects with low parallax uncertainties. The uncertainty in parallax depends on the signal-to-noise ratio, which is correlated with G magnitude, but also on the fact that the star is a binary. Therefore we rejected those stars with error in parallaxes larger than two times the typical error at that G magnitude. Finally, we constrain our analysis to those stars with G magnitude brighter than 18 mag to avoid problems with the completeness of the sample at fainter magnitudes. We have not attempted to use the radial velocities in our analysis because *Gaia* only provides radial velocities for the very bright objects ($G \leq 12$, see Katz et al. 2019; Soubiran et al. 2018) and other studies available in the literature (e.g. Geller et al. 2015) cover areas smaller than that explored in this work.

We used two different methods in order to determine the membership probabilities: *UPMASK* (Unsupervised Photometric Membership Assignment in Stellar Clusters; Krone-Martins & Moitinho 2014) and *Clusterix*² (Balaguer-Núñez et al. 2017) codes. Although *UPMASK* was originally developed to handle photometric data it can be also applied to astrometric data (see the discussion in Cantat-Gaudin et al. 2018b). *UPMASK* assigns the membership probabilities on the basis that member stars must share common properties in μ_{α^*} , μ_{δ} , and ϖ space and are more concentrated in α - δ plane than a random distribution (see Cantat-Gaudin et al. 2018b, for details). On the other hand, *Clusterix* performs an empirical determination of the field and cluster frequency functions in proper motions (μ_{α^*} , μ_{δ}) by comparing two areas: the cluster core and one far enough to represent the field population in the cluster area (see Appendix A for details). For *UPMASK* we considered as cluster members those stars with an astrometric probability, $p \geq 0.4$ (Cantat-Gaudin et al. 2018a; Soubiran et al. 2018). In the case of *Clusterix* we selected as member candidates those objects with $p \geq 0.81$ following the procedure described in Appendix A, applying after an additional constrain in ϖ . *Clusterix* provides a slightly larger number of members than *UPMASK*. Because there is no clear reason to prefer one method over the other, we selected those objects for which both methods agree in labelling them as members. Finally, we fine-tuned the sample on the basis of the positions in the color-magnitude diagram: main-sequence (MS), turn-off (TO), sub giant branch (SGB), red giant branch (RGB), and red clump (RC). Basically, we used the objects inside a radius of $25'$ to define the regions used for this purpose (Fig 1). After all this procedure our sample is formed by 808 objects inside a radius of 150 pc. Following the same procedure we have selected stars redward of the main-sequence in the expected location of the binary sequence. In total there are 144 stars in this region (grey points in Fig. 1).

There are also several stars above the main-sequence turn-off known as blue straggler stars (BSSs, see Fig 1). The formation of these objects is still not well understood but the proposed scenarios include mass transfer or mergers in close binary systems (e.g. McCrea 1964) or collisions between single stars or multiple systems that lead to a merger (e.g. Hills & Day 1976). They are key particles to investigate the internal dynamics because they are typically located in the central regions, probably as a consequence of dynamical friction (e.g. Mapelli et al. 2004). According to Geller et al. (2015, and references therein)

¹ <https://www.cosmos.esa.int/web/gaia/dr2-known-issues>

² Available at <http://clusterix.cab.inta-csic.es/clusterix/>

there are 25 BSS candidates in this cluster (see Table 1). One of these stars, S 1082, is not present in the *Gaia* DR2 catalogue. This is a triple system which includes a RS CVn-type eclipsing binary (Belloni et al. 1998). Both *Clusterix* and *UPMASK* methods yield very low membership probabilities for nine of these stars. Two of them have been discarded on the basis of their radial velocities and the rest are binaries according to Geller et al. (2015). Finally we get a list with eleven BSS candidates with high membership probabilities for the two methods: two of them are new findings of this work in the external regions (see Sect. 3), eight had already been studied by Geller et al. (2015), and the last star, S 1053 is a double-lined spectroscopy binary according to Geller et al. (2015, see Table 1). Seven of the objects in common with Geller et al. (2015) were classified as “single members”, two were marked as “binary likely member” one is the double-lined spectroscopy binary S 1053. The remaining eight BSS candidates has a high membership probability for *Clusterix* but not for *UPMASK*. Five of them are labelled by Geller et al. (2015) as “binary member” or “binary likely member”. In principle this can be explained by the fact that *UPMASK* takes into account the uncertainties in the *Gaia* DR2 astrometric parameters which in principle may be larger for binaries. There is no additional information for the other three previously unstudied objects in the external regions of the cluster. Since there is no additional reason to prefer one over the other, we are going to analyse the *Clusterix* and *UPMASK* BSS samples independently (BSSc and BSSu, respectively).

The stellar sample used in this work, including stellar identification, coordinates and membership probabilities derived by both *UPMASK* and *Clusterix* is only available in electronic form at the CDS.

3. Radial density profile

The radial density profile is a basic tool to investigate the spatial distribution of the cluster stellar populations and their extension. To do that we have calculated the mean stellar surface density in concentric rings as $\rho_i = N_i / \pi(R_{i+1}^2 - R_i^2)$ where N_i is the number of stars in the i -th ring with inner and outer radius R_i and R_{i+1} , respectively. For this purpose we have used only the stars along the cluster sequence, excluding BSS candidates and binaries. The density uncertainty in each ring was estimated assuming Poisson statistics.

The radial density profile obtained is shown in Fig. 2. The stellar density decrease slowly with radius in the inner $\approx 30'$. After this there is a steeper decrease till $\approx 150'$. From there the slope slows down but it does not get flattened since there are still members at larger distances which are not shown in the figure for clarity. The first conclusion is that there are member stars at distances larger than $100'$ (25 pc) from its centre. In fact a preliminary analysis of the *Gaia* DR2 sample showed that the cluster extends at least beyond $\sim 60'$ (≈ 15 pc) from its centre (Gaia Collaboration et al. 2018a). The value found here is much larger than previous determinations in the literature. From 2MASS photometry, Bonatto & Bica (2003) found that the cluster extends up to a distance of about $24'$ (≈ 6 pc) while Davenport & Sandquist (2010), using SDSS photometry, reported that the cluster extends to $\sim 60'$ (≈ 15 pc). More recently, Gao (2018) found a limiting radius of $\sim 62'$ (≈ 16 pc) using also *Gaia* DR2 but using a different method to assign membership probabilities.

In order to characterize the resulting density profile we have fitted it with three different analytic templates: *King* (King 1962); *EFF* (Elson et al. 1987); and *Nuker*

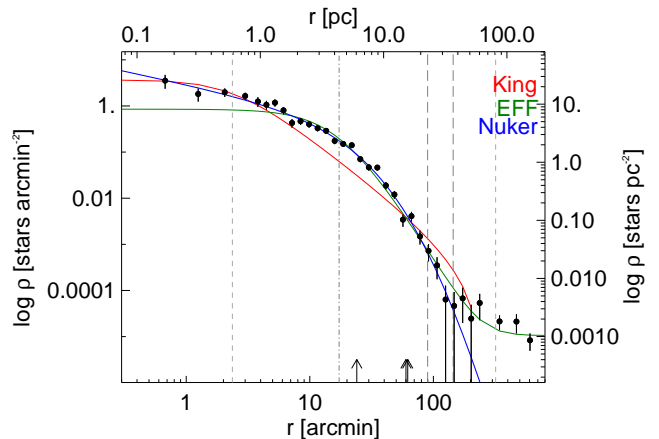


Fig. 2. Stellar radial density profile for M67 members (black filled circles). The different templates fitted have been plotted in different colours (see text for details). Vertical grey lines mark the derived r_c and r_t for *King* (short dashed lines) and *Nuker* (long dashed lines) templates and r_c for *EFF* template (dot-dashed line). Small arrows in the bottom show previous cluster size determinations available in the literature by Bonatto & Bica (2003), Davenport & Sandquist (2010), and Gao (2018) from left to right.

(van der Marel & Anderson 2010). Despite these expressions having been obtained empirically and not being the physical solutions of the collisionless Boltzmann equation, they are useful to analyse the radial density profile. It is assumed that the density profile can be separated in three parts: core, bulk, and halo (or tidal debris). The different templates have been defined to focus on each of these parts. For example, King (1962) tried to reproduce the bulk of the cluster, whereas Elson et al. (1987) focused on the external tidal regions.

In the following we present the analytical templates of the density profiles investigated in this work. A more detailed explanation of each of them is provided by Küpper et al. (2010).

1. The widely used *King* template was presented by King (1962). It is in the form:

$$\rho(r) = \rho_{bg} + \rho_0 \left[\frac{1}{\sqrt{1 + (r/r_c)^2}} - \frac{1}{\sqrt{1 + (r_t/r_c)^2}} \right]^2 \quad (1)$$

where ρ_{bg} is the background density and ρ_0 is the central density. The core radius r_c is defined as the distance between the centre and the point where $\rho(r) = \rho_0/2$. The tidal radius, r_t , is the position where $\rho(r) = \rho_{bg}$, the background density. The King template therefore consists of a flat core and a bulk, but has no term for the tidal debris.

2. Given that the outer parts of the density profiles of several clusters were not properly reproduced by King profiles, Elson et al. (1987), *EFF*, proposed this template which falls like a power-law without edge radius:

$$\rho(r) = \rho_0 \left[1 + \left(\frac{r}{r_c} \right)^2 \right]^{-\eta/2} \quad (2)$$

where ρ_0 , and r_c have the same meaning as in the case of the *King* template. η is the slope of the template for radii much larger than r_c and η is the slope of the template for radii much larger than the core radius.

Table 1. Summary of BSSs

ID ^a	ID ^b	Source_id	distance	Class. ^c	Clusterix	UPMASK	Comments
1006	S1066	604921202767814528	0.05	(BL)M	M	M	SB1,RR,BSS
1007	S1284	604918213470568576	0.06	BM	NM	NM	SB1,RR,EX Cnc,PV,BSS
1010	S977	604911478961895424	0.07	(BL)M	M	NM	RR,BSS,SB1
1017	S1466	604918831945837312	0.14	(S)N	NM	NM	RR,CX109
1020	S751	604914189085426560	0.16	SM	M	M	
1025	S1195	604896566835438464	0.20	BM	M	NM	SB1,RR,BSS
1026	S1434	604903713660959488	0.21	(BL)M	M	M	SB1,RR,BSS
2007	S984	604911337227185920	0.05	SM	M	NM	
2008	S1072	604921374566321920	0.06	BM	NM	NM	SB1,X37,CX24,YG
2009	S1082		0.08	BM			SB2,triple,ES Cnc,X4,CX3,PV,BSS
2011	S968	604910310730777472	0.08	SM	M	M	PV?,BSS
2013	S1267	604918591427681024	0.10	BM	M	NM	SB1,RR,BSS
2015	S792	604921958681906176	0.12	SM	M	M	
2068	S277	604984665204470016	0.56	BM	NM	NM	SB1
3005	S1263	604917835513456512	0.04	SM	M	M	PV,BSS
3009	S1273	604917934296937344	0.07	SM	M	M	
3010	S975	604911268507711232	0.07	BM	NM	NM	SB1,RR,BSS
3013	S752	604911135364519808	0.10	BM	NM	NM	SB1,RR,PV?,BSS
4003	S1036	604918041671889792	0.02	(BL)M	M	NM	SB1,RR,W UMa,EV Cnc,X45,CX19,PV
4006	S1280	604918179110923520	0.05	(BL)M	M	M	SB1,RR,EW Cnc,PV,BSS
5005	S997	604917285757663872	0.03	BM	NM	NM	SB1,CX95,BSS
5071	S145	598958684353074048	0.59	SN	NM	NM	
6038	S2226	604997206508853632	0.31	SM	M	M	BSS
8006	S2204	604917285757665920	0.04	SM	M	M	
9005	S1005	604917560635575808	0.04	BM	NM	NM	SB1
		602049342819274240	1.19		M	M	
3006	S1053	604920923594172928	0.05	BM	M	M	SB2
		578071536838119168	8.85		M	M	
		585923389890240128	9.37		M	NM	
		601873116017045376	2.24		M	NM	
		582587853864423040	7.04		M	NM	

Notes. ^(a) WIYN Open Cluster Study (WOCS) identifier. ^(b) Including red clump. ^(c) Membership classification from Geller et al. (2015) (SM single member; SN single non-member; BM, binary member; BN binary non-member; BLM binary likely member).

3. The *Nuker* template was initially proposed by Lauer et al. (1995) to describe the surface brightness profiles of elliptical galaxies that showed a power-law cusp towards the centre and a logarithmic decline for radii larger than r_c . An additional logarithmic slope from r_t was added by van der Marel & Anderson (2010) in order to describe the surface brightness of ω Centauri. This template is able to fit a cluster with a non-flat core, e.g. a core-collapsed cluster or a cluster with a massive central black hole. It has the form:

$$\rho(r) = \rho_{bg} + \rho_0 2^{\frac{\eta-\gamma}{\alpha}} \left[\frac{r}{r_c} \right]^{-\gamma} \left[1 + \left(\frac{r}{r_c} \right)^{\alpha} \right]^{-\frac{\eta-\gamma}{\alpha}} \left[1 + \left(\frac{r}{r_t} \right)^{\delta} \right]^{-\frac{\epsilon-\eta}{\delta}} \quad (3)$$

where ρ_{bg} , ρ_0 , and r_c are as before. γ and η are the power-law slopes inside and outside r_c , respectively. The factor α smooths the transition between the two slopes. r_t is an additional break radii, from there off the density falls with ϵ logarithmic slope where δ determines the smoothness of the transition between ϵ and η . van der Marel & Anderson (2010) found that the two break radii roughly correspond to the core and tidal radius of the cluster. In brief, this template consists of a flexible core, a bulk and a tidal debris.

Each analytical template has been fitted to the observed profile using a non-linear fitting with the *MPFIT* package

(Markwardt 2009). The best fits in each case have been plotted with different colours in Fig. 2. The *King* template (red line on Fig. 2), consisting of a flat core and a bulk, is only able to reproduce innermost region, $\lesssim 3'$. Up to $\approx 60'$ this template predicts less stars than observed. The *EFF* template (Elson et al. 1987), shown as a green line in Fig. 2, is unable to reproduce the central region, up to $\approx 10'$, predicting fewer stars than actually observed. On the contrary, for larger radii this template reproduces reasonably well the number of stars observed. The modified *Nuker* template proposed by van der Marel & Anderson (2010) is in between of the previous ones. It is able to fit the data with a non-flat core, such as a core-collapsed cluster or a cluster with a massive central black hole. In the case of NGC 2682, this template (blue line in Fig. 2) reproduces the observed stellar density profile almost up to a radius of $\approx 200'$. In the outermost radii the *Nuker* template predicts a continuous logarithmic fall. However, the observed profile shows a change of the slope suggesting the existence of a tidal tail or a halo.

In order to check the statistical significance of the agreement, or disagreement, of the templates and the observed density profile we have computed the χ^2 of the fit in the way

$$\chi^2 = \sum \frac{(\rho_{i,t} - \rho_i)^2}{\sigma_{\rho_i}}$$

where $\rho_{i,t}$ is the density predicted by template t at the i -th ring. We obtained $\chi^2 = 6825.6$, 71.5, and 2.4 for *King*, *EFF*,

Table 2. Summary of cumulative projected radial distribution of different populations.

Population	Nr Stars	$r_{15\%}$	$r_{50\%}$	$r_{85\%}$
All ^a	808	4:7	15:6	37:8
RGB ^b	34	2:1	9:9	28:4
SGB	22	2:3	8:4	29:4
TO	158	2:7	12:5	30:6
MS	594	5:6	17:1	41:5
BSSc	20	2:4	5:2	237:1
BSSu	11	2:4	4:8	60:1
Binaries	144	3:4	12:7	40:5

Notes. ^(a) Does not include BSS and binaries. ^(b) Including Red clump.

and *Nuker* templates, respectively. The values for the best *King* template fit are: $\rho_0 = 3.8 \pm 0.6$ stars arcmin⁻¹; $r_c = 2:4 \pm 0:2$; and $r_t = 319' \pm 9'$. In the case of *EFF* template the best fit is obtained for: $\rho_0 = 0.85 \pm 0.01$ stars arcmin⁻¹; $r_c = 17:27 \pm 0:03$; and $\eta = 4.23 \pm 0.01$. Finally, the values of the best *Nuker* template fit are: $\rho_0 = 6.6 \pm 0.8 \times 10^{-4}$ stars arcmin⁻¹; $r_c = 90' \pm 2'$; $\eta = 10.2 \pm 0.1$; $\gamma = 0.57 \pm 0.01$; $\alpha = 1.14 \pm 0.01$; $r_t = 144' \pm 1'$; $\delta = 28 \pm 4$; and $\epsilon = 3.1 \pm 0.1$. The *Nuker* template reproduced better than the other the observed stellar density profile for NGC 2682 as the χ^2 value confirms.

Figure 3 shows the cumulative projected radial distribution of the different NGC 2682 stellar populations normalised to the total number of the sub-population and including BSS and binaries. It is clear that the global distribution (open black circles) is mainly due to the MS stars (magenta squares) particularly in the outskirts. Turn-off objects (green squares) follow a similar trend than MS ones but they are more concentrated. While the 15% of the MS population is located inside a radius, $r_{15\%}$, of 5:6 the TO is concentrated inside 2:7 (see Table 2). In fact, the $r_{15\%}$ increases when we go down in the cluster sequence. The same trend is observed for $r_{85\%}$, the radius that contains the 85% of the stars of a given population. The binaries (grey stars in Fig. 3) are slightly more concentrated than the MS objects as expected since they may be more massive objects. Since the mass of the star decreases as we go fainter along the cluster sequence the observed trend confirms that this cluster is mass-segregated with the most massive objects concentrated in the central regions. This behaviour has been reported in the literature by several authors (e.g. Balaguer-Núñez et al. 2007; Geller et al. 2015; Gao 2018).

The distribution of the BSS deserves a more detailed analysis. In principle, both *Clusterix*, blue upward triangles in Fig. 3, and *UPMASK*, cyan downward triangles in Fig. 3, samples shows a similar trend. The bulk of the BSS are confined in the central regions of the clusters with the 50% of the population inside $r_{50\%} \sim 5'$ (see Table 2). There is a fraction of BSSs at large radii although they need to be confirmed as really BSS objects. Between $\approx 10'$ and $100'$ there are almost no BSSs. This trend with the majority of the objects in the central region and several in the outskirts with almost none of them in between has been reported in globular clusters (e.g. Ferraro et al. 1997; Lanzoni et al. 2007). The observed distribution could be due to the BSS formation mechanism as suggested by dynamical simulations (Mapelli et al. 2004). The objects in the external regions would be the result of mass transfer in primordial binaries where BSSs in the cluster core have most likely a collisional origin.

4. Three-dimensional spatial distribution

In order to further investigate the outskirts of NGC 2682 we have derived its 3D spatial distribution. Without observational uncertainties on the parallaxes the individual distances could be simply obtained as the inverse of the parallax, $d = \varpi^{-1}$. However, observational errors on measured parallaxes are not negligible and their direct propagation to distances through inversion may yield unacceptable results, that would translate into a strong elongation of the three-dimensional shape along the line of sight (Smith & Eichhorn 1996; Bailer-Jones 2015; Luri et al. 2018). To overcome this difficulty, we used a Bayesian approach to parallax inversion described in Appendix B, essentially following Bailer-Jones (2015) but with a different prior, which combines two terms: the cluster proper, or core, and a field/halo term which accounts for stars that either form a diffuse envelope around the cluster or are serendipitously placed at a similar distance and share proper motions with the cluster. The first term is represented by a normal distribution for simplicity and the second term is the exponentially decreasing volume density prior introduced by Bailer-Jones (2015). A detailed analysis of the prior that is best for clusters is out of the scope of this paper. In our case the form of the prior does not have a big impact since the main result comes without 3D information, i.e. the sky-projected positions of stars which do not depend on parallaxes but shows a small tail in the opposite direction to that of the movement (top right panel of Fig. 4). On the other hand, if the parallaxes are giving us enough information then the shape of prior does not make a large difference unless it is very unrealistic.

The distribution of NGC 2682 in Galactic cartesian coordinates is shown in Fig. 4. In this coordinate system, the *X* axis points towards the Galactic centre, *Y* is positive towards the local direction of rotation in the plane of the Galaxy, and *Z* points towards the North Galactic Pole. The Galactic centre is the origin of this system with the Sun located at (-8340,0,27) pc (see Katz et al. 2019, and references therein). The spatial distribution of the stars is not isotropic in the *XZ*- and *ZY*-planes despite the symmetric nature of the normal term representing the cluster in the prior. This is a clear indication that the observed parallaxes have a non-negligible effect on the posterior. In the case of the *XZ*-plane (top left panel), there is a clear tail almost in the direction opposite to that of the cluster's movement. An elongation is observed in the direction of the movement in the *ZY*-plane (bottom right panel). A small elongation is also observed in the *XY*-plane (bottom left panel), but in this case in the direction perpendicular to the movement.

Davenport & Sandquist (2010) using ground based photometry reported an asymmetric halo up to a distance of $60'$ from the cluster centre elongated roughly in-line with the proper-motion vector on the sky plane (see Fig 10 of Davenport & Sandquist 2010). However, such elongation is not observed in our case (top right panel of Fig. 4). However, as commented before a small tail is visible in the opposite direction to that of the movement.

5. Physical interpretation

We estimate the radius of NGC 2682's Hill sphere R_H in the Galactic potential by approximating the latter to a point-particle potential, obtaining

$$R_H = D \times \left(\frac{m}{3M} \right)^{1/3} \quad (4)$$

where D is the distance of NGC 2682 from the Galactic centre, m the mass of NGC 2682, and M the mass of the Galaxy

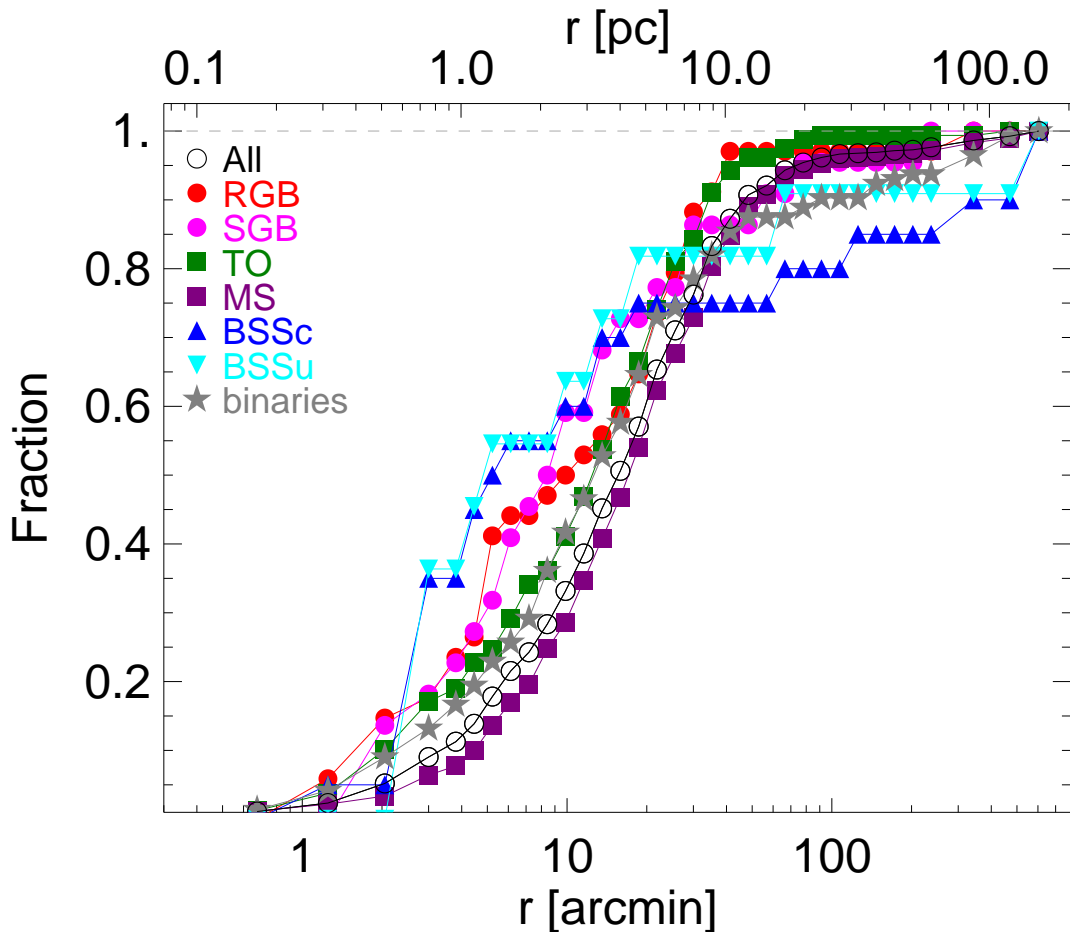


Fig. 3. Cumulative projected radial distribution of different populations identified in NGC 2682 normalised to the total number of stars in each population. Errorbars have not been plotted for clarity.

enclosed within NGC 2682 orbit. The quantity we know with less uncertainty is D , which is estimated as $D = 8.9$ kpc from *Gaia* DR2 (Cantat-Gaudin et al. 2018a). On the other hand, the total mass of the Galaxy is model dependent, e.g. $M = 10^{12} M_{\odot}$ (McMillan 2017) and this uncertainty is compounded by the fact that we want to consider only the mass within NGC 2682 orbit. Similarly, there is likely an uncertainty of a factor 2 in estimates of NGC 2682 mass such as Hurley et al. (2005) which sets it at $m = 2 \times 10^3 M_{\odot}$. Luckily, the dependence to the power of $1/3$ in Eq. 4 ensures that the uncertainty on these numbers has little effect on R_H . To illustrate this, let us consider two different extreme scenarios:

- Overestimate the enclosed Galactic mass at $M = 10^{12} M_{\odot}$ and underestimate NGC 2682 mass at $m = 10^3 M_{\odot}$, obtaining $R_H = 6.2$ pc
- Underestimate the enclosed Galactic mass at $M = 10^{11} M_{\odot}$ and overestimate NGC 2682 mass at $m = 10^4 M_{\odot}$, obtaining $R_H = 28.6$ pc

In both cases, our observations show that M67 stars can be found further out than R_H , suggesting that they are indeed extra-tidal. Such loosely bound stars may have originated as the consequence of internal relaxation (i.e. they may be dynamically evaporated stars) or as the effect of an external disturbance.

We used the software *GRAVPO16* (Fernandez-Trincado 2017; Robin et al. 2012, 2003) to integrate the orbit of NGC 2682 back in time for 1 Gyr. We find that the last disk passage of NGC 2682 happened ≈ 40 Myr ago, as shown in Fig. 5

which plots the height over the Galactic plane Z as a function of time in the last 200 Myr. The shadow region shows the width of the thin disk according to Jurić et al. (2008). Note that the thick disk width is larger than the area plotted. This result is qualitatively compatible to the findings of Pichardo et al. (2012), even though the exact time of last crossing differs due to systematics introduced by the usage of different Galactic potential models and to the lack of good proper motions in the pre-*Gaia* era.

According to Hurley et al. (2005) the relaxation time of a realistic N -body model of NGC 2682 was initially (before mass loss) ≈ 300 Myr. Even allowing for mass loss shortening the relaxation time by a factor ten, it is reasonable to assume that the effects of this disk passage have not yet been erased by dynamical relaxation, especially in the external regions of the clusters where the relaxation time is shorter than the half-light relaxation time. According to Fig. 5 NGC 2682 has had three crossing disk passages in the last 200 Myr which implies that the cluster is constantly disturbed and it will never be relaxed because the frequent passages.

The extra-tidal features we observe in M67 would thus be quite a natural result of disk shocking. This is to be confirmed quantitatively with dedicated N -body models in an upcoming paper (Pasquato et al. 2019, in preparation).

An estimate of the effects of disk crossing can be obtained in the analytical approximation of an impulsive shock

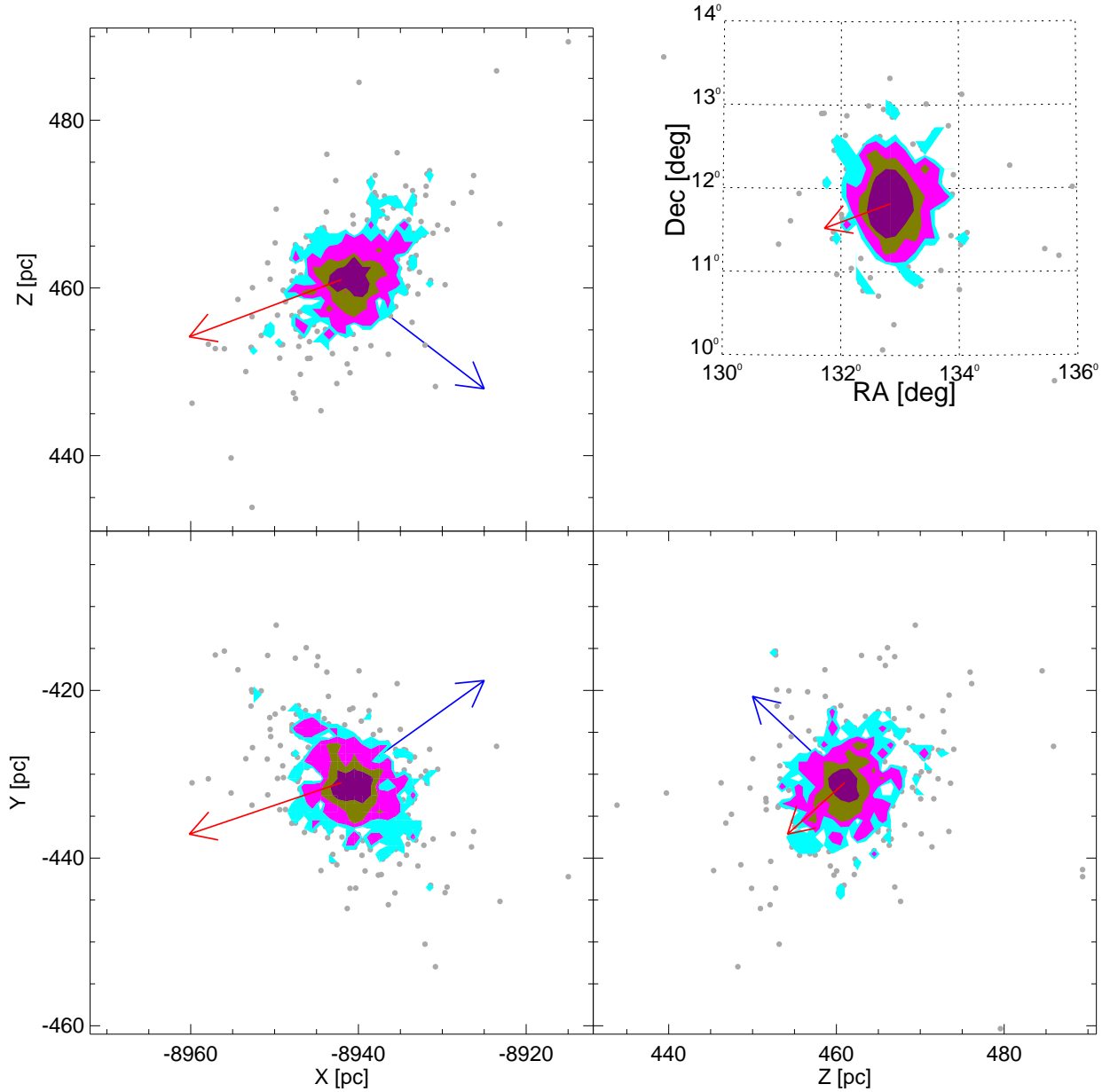


Fig. 4. Position of the M67 members in the Galactic Cartesian coordinates (grey dots). Contours show different stellar densities. Red arrows are proportional to the velocities in each axis derived by Soubiran et al. (2018). Blue arrows show the direction to the observer.

(Ostriker et al. 1972), where every star gets a nudge in velocity

$$\delta v_z = \frac{4\pi G \Sigma z}{V} \quad (5)$$

where V is the velocity with which the cluster crosses the disk, z is the distance along the Z coordinate of a given star from the cluster centre, and Σ is the density per unit surface of the Galactic disk. This corresponds, for a typical star moving with velocity $v = GM/R_h$ relative to the cluster centre, to a relative change in energy of order

$$\frac{\delta E}{E} = \frac{\delta v_z^2}{v^2} \approx \frac{16\pi^2 G \Sigma^2 R_{mh}^3}{M V^2} \quad (6)$$

where R_h is the cluster's half-mass radius, and M the total mass of the cluster. This is proportional to $M_D^2 \sigma^2 / M^2 V^2$ where M_D is the mass enclosed, on the galactic disk, by a circumference with radius the cluster's half-mass radius, and σ is the cluster's velocity dispersion.

Based on our orbital calculations, $V \approx 30 \text{ km s}^{-1}$, and a surface mass density of $30 M_\odot \text{ pc}^{-2}$ (McGaugh 2016) we obtain $\delta E/E \approx 0.3$, which corresponds to an expansion of the virial radius of the cluster of the same quantity, i.e. $\delta R/R \approx \delta E/E \approx 0.3$. This is enough to justify the presence of a relatively large number of extratidal stars.

6. Conclusions

Two different methods, *Clusterix* and *UPMASK* have been used to assign membership probabilities to stars in the line of sight of NGC 2682 up to a distance of 150 pc (10 degrees) using the information provided by the *Gaia*-DR2 catalogue. Additionally, we have estimated distances to obtain three-dimensional stellar positions using a Bayesian approach to parallax inversion, with an appropriate prior for star clusters. The main results of our analysis are:

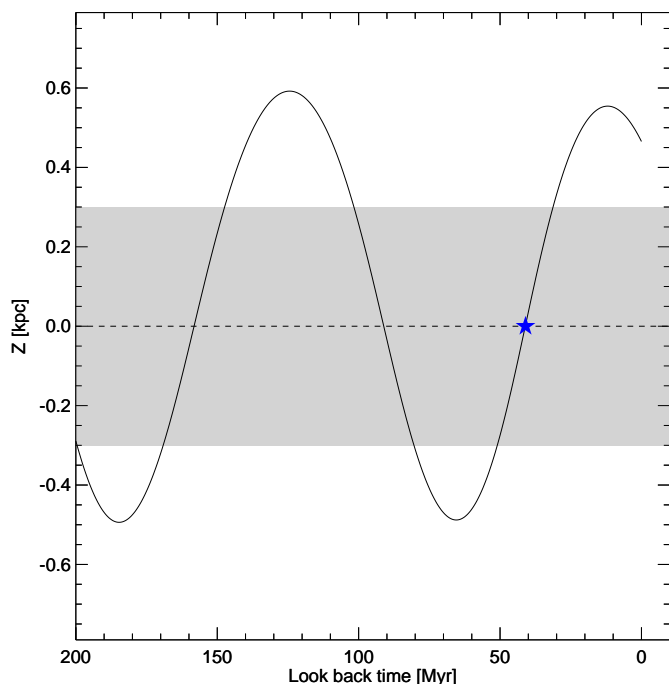


Fig. 5. Height on the Galactic plane Z as a function of time in the last 200 Myr of the orbit of NGC 2682 as integrated by *GRAVOT16*. The green star shows the time of the last disk passage ≈ 40 Myr ago. The shadow area shows the extension of the thin disk.

- The cluster extends up to $200'$ (50 pc) which implies that its size is at least twice as previously believed. This exceeds the cluster Hill sphere based on the Galactic potential at the distance of NGC 2682.
- Only a template with a power-law cusp towards the centre and a logarithmic decline for larger radii is able to reproduce the observed stellar density profile. In any case, there are stars outside the tidal radius.
- As reported in previous studies, we confirm that the cluster is mass-segregated with the most massive objects concentrated in the central regions.
- As observed in several globular clusters the BBSs show a bimodal distribution with the majority of the object located in the core and several objects in the outskirts without anything in between. Although the objects at larger radii need to be confirmed as real BBSs.
- The extra-tidal stars in NGC 2682 may originate from external perturbations such as disk shocking or dynamical evaporation from two-body relaxation. The former origin is plausible given the orbit of NGC 2682, which crossed the Galactic disk ≈ 40 Myr ago. We plan to further investigate this scenario with direct N-body models.

Acknowledgements. This work has made use of data from the European Space Agency (ESA) mission *Gaia* (<https://www.cosmos.esa.int/gaia>), processed by the *Gaia* Data Processing and Analysis Consortium (DPAC, <https://www.cosmos.esa.int/web/gaia/dpac/consortium>). Funding for the DPAC has been provided by national institutions, in particular the institutions participating in the *Gaia* Multilateral Agreement. This project has received funding from the European Union's Horizon 2020 research and innovation programme under the Marie Skłodowska-Curie grant agreement No. 664931. This work was partly supported by the MINECO (Spanish Ministry of Economy) through grant ESP2016-80079-C2-1-R (MINECO/FEDER, UE) and MDM-2014-0369 of ICCUB (Unidad de Excelencia 'María de Maeztu'), European Community's Seventh Framework Programme (FP7/2007-2013) under grant agreement GENIUS FP7 - 606740 and the European Commission Framework Programme Horizon 2020 Research and Innovation action under grant agreement ASTERICS 653477. Support from PREMIALE 2016 MITIC is acknowledged.

Based on Clusterix 2.0 service at CAB (INTA-CSIC). DB is supported in the form of work contract FCT/MCTES through national funds and by FEDER through COMPETE2020 in connection to these grants: *UID/FIS/04434/2019*; *PTDC/FIS - AST/30389/2017&POCI - 01 - 0145 - FEDER - 030389*

References

- Arenou, F., Luri, X., Babusiaux, C., et al. 2018, *A&A*, 616, A17
- Bailer-Jones, C. A. L. 2015, *Publications of the Astronomical Society of the Pacific*, 127, 994
- Balaguer-Núñez, L., Galadí-Enríquez, D., & Jordi, C. 2007, *A&A*, 470, 585
- Balaguer-Núñez, L., Galadí-Enríquez, D., López del Fresno, M., et al. 2017, in *Highlights on Spanish Astrophysics IX*, ed. S. Arribas, A. Alonso-Herrero, F. Figueras, C. Hernández-Monteagudo, A. Sánchez-Lavega, & S. Pérez-Hoyos, 328–333
- Bastian, N. & Gieles, M. 2008, in *Astronomical Society of the Pacific Conference Series*, Vol. 388, *Mass Loss from Stars and the Evolution of Stellar Clusters*, ed. A. de Koter, L. J. Smith, & L. B. F. M. Waters, 353
- Baumgardt, H. & Makino, J. 2003, *MNRAS*, 340, 227
- Belloni, T., Verbunt, F., & Mathieu, R. D. 1998, *A&A*, 339, 431
- Binney, J. & Tremaine, S. 1987, *Galactic dynamics*
- Bonatto, C. & Bica, E. 2003, *A&A*, 405, 525
- Bossini, D., Vallenari, A., Bragaglia, A., et al. 2019, *A&A*, 623, A108
- Cantat-Gaudin, T., Jordi, C., Vallenari, A., et al. 2018a, *A&A*, 618, A93
- Cantat-Gaudin, T., Vallenari, A., Sordo, R., et al. 2018b, *A&A*, 615, A49
- Davenport, J. R. A. & Sandquist, E. L. 2010, *ApJ*, 711, 559
- Dias, W. S., Alessi, B. S., Moitinho, A., & Lépine, J. R. D. 2002, *A&A*, 389, 871
- Elson, R. A. W., Fall, S. M., & Freeman, K. C. 1987, *ApJ*, 323, 54
- Fan, X., Burstein, D., Chen, J.-S., et al. 1996, *AJ*, 112, 628
- Fernandez-Trincado, J. G. 2017, PhD thesis
- Ferraro, F. R., Paltrinieri, B., Fusi Pecci, F., et al. 1997, *A&A*, 324, 915
- Fürnkranz, V., Meingast, S., & Alves, J. 2019, *arXiv e-prints* [arXiv:1902.07216]
- Gaia Collaboration, Babusiaux, C., van Leeuwen, F., et al. 2018a, *A&A*, 616, A10
- Gaia Collaboration, Brown, A. G. A., Vallenari, A., et al. 2018b, *A&A*, 616, A1
- Gaia Collaboration, Prusti, T., de Bruijne, J. H. J., et al. 2016, *A&A*, 595, A1
- Galadí-Enríquez, D., Jordi, C., & Trullols, E. 1998, *A&A*, 337, 125
- Gao, X. 2018, *ApJ*, 869, 9
- Geller, A. M., Latham, D. W., & Mathieu, R. D. 2015, *AJ*, 150, 97
- Gieles, M., Portegies Zwart, S. F., & Athanassoula, E. 2009, *The Effect of Giant Molecular Clouds on Star Clusters*, ed. T. Richtler & S. Larsen, 375
- Hills, J. G. & Day, C. A. 1976, *Astrophys. Lett.*, 17, 87
- Hurley, J. R., Pols, O. R., Aarseth, S. J., & Tout, C. A. 2005, *MNRAS*, 363, 293
- Jurić, M., Ivezić, Z., Brooks, A., et al. 2008, *ApJ*, 673, 864
- Katz, D., Sartoretti, P., Cropper, M., et al. 2019, *A&A*, 622, A205
- Kharchenko, N. V., Piskunov, A. E., Schilbach, E., Röser, S., & Scholz, R.-D. 2013, *A&A*, 558, A53
- King, I. 1962, *AJ*, 67, 471
- Krone-Martins, A. & Moitinho, A. 2014, *A&A*, 561, A57
- Küpper, A. H. W., Kroupa, P., Baumgardt, H., & Heggie, D. C. 2010, *MNRAS*, 401, 105
- Lamers, H., Gieles, M., Bastian, N., et al. 2005, *Astronomy & Astrophysics*, 441, 117
- Lanzoni, B., Dalessandro, E., Ferraro, F. R., et al. 2007, *ApJ*, 663, 267
- Lauer, T. R., Ajhar, E. A., Byun, Y.-I., et al. 1995, *AJ*, 110, 2622
- Lindgren, L., Hernández, J., Bombrun, A., et al. 2018, *A&A*, 616, A2
- Liu, F., Asplund, M., Yong, D., et al. 2016, *MNRAS*, 463, 696
- Luri, X., Brown, A. G. A., Sarro, L. M., et al. 2018, *A&A*, 616, A9
- Mapelli, M., Sigurdsson, S., Colpi, M., et al. 2004, *ApJ*, 605, L29
- Markwardt, C. B. 2009, in *Astronomical Society of the Pacific Conference Series*, Vol. 411, *Astronomical Data Analysis Software and Systems XVIII*, ed. D. A. Bohlender, D. Durand, & P. Dowler, 251
- McCrea, W. H. 1964, *MNRAS*, 128, 147
- McGaugh, S. S. 2016, *ApJ*, 816, 42
- McMillan, P. J. 2017, *MNRAS*, 465, 76
- Meingast, S. & Alves, J. 2019, *A&A*, 621, L3
- Ostriker, J. P., Spitzer, Jr., L., & Chevalier, R. A. 1972, *ApJ*, 176, L51
- Pichardo, B., Moreno, E., Allen, C., et al. 2012, *The Astronomical Journal*, 143, 73
- Pichardo, B., Moreno, E., Allen, C., et al. 2012, *AJ*, 143, 73
- Robin, A. C., Marshall, D. J., Schultheis, M., & Reylé, C. 2012, *A&A*, 538, A106
- Robin, A. C., Reylé, C., Derrière, S., & Picaud, S. 2003, *A&A*, 409, 523
- Röser, S. & Schilbach, E. 2019, *arXiv e-prints* [arXiv:1903.08610]
- Röser, S., Schilbach, E., & Goldman, B. 2019, *A&A*, 621, L2
- Smith, Haywood, J. & Eichhorn, H. 1996, *MNRAS*, 281, 211
- Soubiran, C., Cantat-Gaudin, T., Romero-Gómez, M., et al. 2018, *A&A*, 619, A155
- Spitzer, Lyman, J. 1958, *ApJ*, 127, 17
- Spitzer, L. 1987, *Dynamical evolution of globular clusters*
- van der Marel, R. P. & Anderson, J. 2010, *ApJ*, 710, 1063
- Yeh, F. C., Carraro, G., Montalto, M., & Seleznev, A. F. 2019, *AJ*, 157, 115

Appendix A: Clusterix membership selection

Clusterix is a web-based tool for the determination of membership probabilities from proper motion data using a non-parametric approach based on the formalism described by Galadi-Enriquez et al. (1998), in a new implementation whose details can be found in Balaguer-Núñez et al. (2017). In the sky area occupied by the cluster, the frequency function is assumed to be made up from two contributions: cluster and field stars. The tool performs an empirical determination of the frequency functions from the vector-point diagram (VPD) without relying on any previous assumption about their profiles. To disentangle the two populations, *Clusterix* studies the VPD corresponding to two areas on the plane of the sky: one in the cluster core and another one far enough from the cluster to have a small (negligible) cluster contribution, but close enough to still be a good representation of the field in the cluster area. *Clusterix* allows to search in an interactive and visual way the appropriate areas until an optimal separation is obtained (more details will be given in Balaguer-Núñez et al, in preparation). Several limits can be adjusted to make the calculation computationally feasible without interfering in the quality of the results: in this case we have set a constrain in proper motions ($-15 \leq \mu_{\alpha*} \leq +15$ and $-15 \leq \mu_{\delta} \leq +15$ mas yr⁻¹), proper motions errors (below 5 mas yr⁻¹) and magnitude ($G < 18$). Given that the *Clusterix* selection is only based on proper motions we added an additional constrain in parallaxes choosing only those objects within $\pm 2\sigma$ from the median of the ϖ distribution. The current version of *Clusterix* does not apply any criteria based on spatial distribution nor photometry for membership assessment.

There is no rigorous way to decide where to set the limit between members and non-members in a list sorted by membership probabilities. This non-parametric membership method produces an expected number of cluster members that serves as an indication of the probability limit for the most probable cluster members. However, when the study is done over a large sky area, as in this case, the field surrounding the cluster cannot be considered perfectly homogeneous, due to the existence of other structures in the background and surroundings (e.g. other clusters). This is not a problem for the calculation of the membership, as long as the area chosen to represent the cluster is not too far from the cluster core, but it has an impact on the calculation of the expected number of cluster members, as this quantity depends on the total number of stars in the area. In this case, we have performed this study in two steps: first considering an area of 5 deg where the field is homogeneous enough and the number of expected cluster members gives a reliable result, followed by a second step, using that list of members (where most of the cluster is found) to fix the membership probability cut on the study of the 10 deg area ($p \geq 0.81$).

Appendix B: Bayesian inference of stellar distances for reconstructing the 3D shape of NGC 2682

As commented in Sect. 4 the propagation of the non negligible ϖ uncertainties causes that the determination of distances through the inversion of the parallax, $d = \varpi^{-1}$, produces erroneous results. In order to overcome this issue we have used a Bayesian approach to determine distances, d , to the objects analysed in this paper. To do that we follow Bailer-Jones (2015) Bayesian approach, using for each star the parallax ϖ to update a prior distribution in distance $\Pi(d)$, obtaining an (un-normalized) posterior distribution as follows:

$$f(d|\varpi) \propto f(\varpi|d)\Pi(d) \quad (\text{B.1})$$

where

$$f(\varpi|d) \propto e^{-(\varpi - \frac{1}{d})^2 / 2\sigma_{\varpi}^2} \quad (\text{B.2})$$

with σ_{ϖ}^2 equal to the quoted error bar on each parallax measurement, i.e. we assumed that uncertainties on the parallax are Gaussian, with a standard deviation equal to the quoted error bar σ_{ϖ} . Regarding the prior, we used a Gaussian centred at the average distance of NGC 2682, $d_0 \approx 860$ pc (Cantat-Gaudin et al. 2018a) to represent the cluster, plus a term that accounts for field stars or more in general stars that may be forming a diffuse envelope around NGC 2682, for which we do not wish to make overly restrictive assumptions. The standard deviation of the Gaussian term, σ_d was chosen equal to the standard deviation of physical distances of member stars projected on the plane of the sky. This is equivalent to assuming, in the prior, that the cluster term is spherical. While the choice of a Gaussian prior may seem unjustified from the physical point of view we chose it for simplicity, as it is significantly easier to implement than e.g. a King model. The resulting prior is as follows:

$$\Pi(d) = \alpha \xi(d) + (1 - \alpha) \frac{1}{\sqrt{2\sigma_d}} e^{-(d-d_0)^2 / 2\sigma_d^2} \quad (\text{B.3})$$

where $\xi(r)$ is a (normalized) exponentially decreasing volume density prior (see Eq. 17 of Bailer-Jones 2015, with $L=8$ kpc), and $1-\alpha$ is the *UPMASK* membership score. As the Bailer-Jones (2015) prior is essentially a smoothly truncated constant density prior it is a good choice for not making strong assumptions about the start that happen to be loosely associated to NGC 2682. The adopted distance for each star is estimated with the mode of the posterior distribution. As pointed out in Luri et al. (2018), the whole posterior distribution should be kept, rather than summarized, as the end result of a correct Bayesian inference procedure. This applies in our case a fortiori, because we are not interested in the position of individual stars as much as we are interested in the overall mass density distribution of the whole cluster. However in this letter, for the sake of concreteness, we decided to obtain anyway a point estimate from the posterior distribution.